Phonons and superconductivity in $YBa_2Cu_3O_7$

G. L. Zhao and J. Callaway
Department of Physics and Astronomy, Louisiana State University, Baton Rouge, Louisiana 70803-4001
(Received 22 February 1994; revised manuscript received 12 May 1994)

We report the results of a calculation of the electron-phonon interaction in $YBa_2Cu_3O_7$ based on the nonorthogonal tight-binding approach to lattice dynamics. A self-consistent local-density electronic-structure calculation was combined with a shell-model description of the phonon spectrum. The resulting interaction matrix was used to calculate the superconducting transition temperature from a solution of the Eliashberg equations in which the full **k** dependence was retained. The transition temperature was found to be about 90 K, quite close to experiment. The oxygen isotope effect was investigated. We also calculated the **k**-dependent gap function at $T=0$. The gap shows significant variation between different sheets of the Fermi surface as well as dependence on **k** on the individual sheets, but is nodeless. The quantity $2\Delta/k_BT_c$ varies from 6.0 to 2.5 on the Fermi surface.

I. INTRODUCTION

The role of the electron-phonon (*e*-ph) interaction in high-temperature cuprate superconductors is not understood; it has been, and still is, a subject of controversy. Basic observations made quite early in the development of this subject led many to conclude that phonons could not be very important, especially in $YBa_2Cu_3O_7$ and other members of the cuprate family with T_c's between 80 and 150 K. Some reasons for this opinion will be discussed briefly below. As a result, there has been an intensive search for other interactions of electronic origin. Although there are numerous proposals of alternatives, there is so far no general agreement as to the origin of high T_c. In this paper, we report the results of a calculation of T_c in $YBa_2Cu_3O_7$ and of the gap function at $T=0$ using a realistic band structure and phonon spectrum, assuming that it is the electron-phonon interaction which produces superconductivity in this material. In contrast to a previous calculation, we find that T_c agrees reasonably well with experiment. At $T=0$, we find an anisotropic (but nodeless) energy gap with significantly different values on different sheets of the Fermi surface. A brief outline of these findings was reported previously.[1] The present paper is intended to give a more complete account of our calculation.

The belief that phonons could not be responsible for the high-T_c superconductivity of the cuprates is based on many considerations: all plausible; none really conclusive. In the first place, the magnitude of T_c itself is much larger than previous experience with more conventional materials, where the superconductivity is known to result from the electron-phonon interactions, had suggested might be achievable. However, the Eliashberg theory, which is the basis of the calculation of T_c, does not imply a fundamental limit on T_c, provided that the interaction (whose strength is conventionally measured by a parameter λ) is strong enough.[2]

Could the electron-phonon interaction be strong enough to yield a T_c around 90 K? According to Carbotte,[3] if electrons can interact strongly with phonons of an optimum frequency, then $T_c \sim \frac{2}{15}\omega$ is reasonable. The phonon spectrum of $YBa_2Cu_3O_7$ extends up to about 80 meV, so that it is quite reasonable to consider superconductivity based on the electron-phonon interactions. However, there are important and still unresolved difficulties with this view. One is associated with nearly linear temperature dependence of the electrical resistivity in the normal state, which is asserted to be incompatible with strong electron coupling to high-energy phonons.[4] The other is the smallness of the observed oxygen isotope effect.[5] Although a small isotope effect may be consistent with an electron-phonon interaction, it has been argued that the combination of high T_c and small isotope effect rules out the electron-phonon interaction as the sole source of pairing.[6] Here also, the argument is not conclusive: a small isotope effect is possible if anharmonic effects are important.[7]

In contrast to these arguments, there are observations which point toward strong electron-phonon coupling. For example, temperature-dependent studies of the channeling of energetic ions in single crystals of $YBa_2Cu_3O_7$ (YBCO) reveal an abrupt change in the displacements in the *a-b* plane of Cu(1), Cu(2), and O(4) atoms on passing through T_c.[8] Raman scattering measurements have shown that some phonons in YBCO soften as the temperature is decreased through T_c.[9] Observations of structure in the tunneling conductance of YBCO can be interpreted as indicating strong electron-phonon coupling.[10]

We now turn to a consideration of some previous calculations of the electron-phonon interaction in $YBa_2Cu_3O_7$. Rather early in the development of this subject, the interaction was studied by Weber and Mattheiss[11] based on a tight-binding fit to a previously calculated band structure[12] and the nonorthogonal tight-binding (NTB) model of lattice dynamics.[13] These authors concluded that the electron-phonon coupling is small in the $pd\sigma$ band close to the Fermi energy. They did not give a specific calculated value of T_c, but presented a range of possible values ranging from 3 up to 30 K

depending on specific procedures and allowances for possible omissions in their computations.

However, the band structure of YBCO shown in Ref. 12 differs significantly from the results of more recent investigations.[14] Also, the phonon density of states shown in Ref. 11 seems to have significantly less weight at high frequencies than is found in other calculations.[15] More recently, two other groups have studied the electron-phonon interaction in YBCO using the frozen-phonon method and density-functional theory,[16,17] and have found relatively strong interactions for Raman-active phonons. However, the frozen-phonon method can be used only at symmetry points of the zone, and does not give the complete phonon spectrum.

We have chosen to concentrate on $YBa_2Cu_3O_7$ in this work because optimum superconductivity occurs at or close to the stoichiometric composition. It is a well characterized material, and the crystal structure is manageable from the point of view of electronic-structure computations. We do not wish to consider the problems associated with the disordered potentials of randomly substituted ions, which arise in the case of doped La_2CuO_4. Most of the materials with T_c's appreciably higher than that of $YBa_2Cu_3O_7$ are also quite significantly more complicated from a computational point of view. We assume that YBCO is a conventional but complicated metal. It is conventional in that electrons form a Fermi liquid. It is complicated in that the complex band structure resulting from local-density band calculations must be seriously considered.

We have calculated T_c in $YBa_2Cu_3O_7$ using the strong-coupling Eliashberg theory. In contrast to much previous work, we make full allowance for anisotropy. In addition, we have calculated the complex gap functions on different sheets of the Fermi surface at $T=0$. These calculations are also performed using the anisotropic Eliashberg equations (but with real frequencies). We find a high T_c consistent with experiment and a highly anisotropic but nodeless gap function.

Our calculations are based on a self-consistent local-density electronic-structure calculation which was performed using a linear combination of atomic orbitals (LCAO) method.[18] This procedure has been tested by ourselves and others and found to give results of comparable accuracy to those obtained by other first-principles methods.[19–21] In particular, the YBCO band structure agrees satisfactorily with the results of other recent calculations,[17] and with measurements of the Fermi surface by angle-resolved photoemission.[22–24] We also require both phonon frequencies and phonon eigenvectors throughout the Brillouin zone. In order that these should be as close to experiment as practical, we made a shell-model calculation employing parameters determined by Humlicek *et al.*[25] through a fit to the observed Raman spectra.

The remainder of this paper is organized as follows. The next section (II) lists the basic equations, which we solve to find T_c, and also the gap function at $T=0$. Our calculational procedures are summarized in Sec. III. The results for T_c are presented in Sec. IV, which also contains some discussion of the oxygen isotope effect. Our results for the gap function are contained in Sec. V. The paper ends with concluding remarks in Sec. VI.

II. DESCRIPTION OF SUPERCONDUCTIVITY

We followed the standard procedures of the strong-coupling (Eliashberg) theory in calculating T_c and the gap function at $T=0$. However, we think that our work may be an improvement over what has been done previously in that we take full account of anisotropy, which means that the complete wave-vector dependence of the coupling is included.

The transition temperature T_c was calculated using the anisotropic Eliashberg equations with imaginary frequencies as given by Allen and Mitrovic.[2] Local-density calculations show that the Fermi surface has sheets in four bands. Therefore we consider both the gap function Δ and the renormalization function Z to have components in these bands, and they are labeled by a band index. The equations which determine the functions $\Delta_m(\mathbf{k},i\omega_n)$, and the renormalization function $Z_m(\mathbf{k},i\omega_n)$ are

$$\Delta_m(\mathbf{k},i\omega_n)Z_m(\mathbf{k},i\omega_n)=\pi T\sum_{m'\mathbf{k}'n'}^{|\omega_{n'}|<\omega_c}\frac{\delta(E_{m'\mathbf{k}'})}{N(0)|\omega_{n'}|}\{\lambda(m\mathbf{k},m'\mathbf{k}';n-n')-\mu^*(\omega_c)\}\Delta_{m'}(\mathbf{k}',i\omega_{n'}) , \quad (1)$$

and

$$Z_m(\mathbf{k},i\omega_n)=1+\frac{\pi T}{|\omega_n|}\sum_{m'\mathbf{k}'n'}^{|\omega_{n'}|<\omega_c}\frac{\delta(E_{m'\mathbf{k}'})}{N(0)}\times\{\lambda(m\mathbf{k},m'\mathbf{k}';n-n')\}s_n s_{n'} , \quad (2)$$

in which

$$\lambda(m\mathbf{k},m'\mathbf{k}';\nu)=\sum_{\mu}2N(0)|g_{m\mathbf{k},m'\mathbf{k}',\mu}|^2\times\omega_\mu(\mathbf{k}-\mathbf{k}')/[\omega_\nu^2+\omega_\mu^2(\mathbf{k}-\mathbf{k}')] . \quad (3)$$

In these equations, the electron states of energies $E_{m\mathbf{k}}$ and $E_{m'\mathbf{k}'}$ are on the Fermi surface; $N(0)$ is the density of states per spin at the Fermi energy;

$$s_n\equiv\mathrm{sgn}(\omega_n)=(n+\tfrac{1}{2})/|n+\tfrac{1}{2}| ;$$

$\mu^*=U_cN(0)$ is the parameter of the pseudo-Coulomb interaction; $\omega_n=(2n+1)\pi T$; and $\omega_\nu=2\pi\nu T$. The electron-phonon coupling is described by the quantities $g_{m\mathbf{k},m'\mathbf{k}',\lambda}$.

The quantities are calculated according to the nonorthogonal tight-binding theory of lattice dynamics.[13]

$$g_{m\mathbf{k},m'\mathbf{k}'\lambda}=\sum_{\kappa\alpha}[\hbar/2M_\kappa\omega_\lambda(\mathbf{k}-\mathbf{k}')]^{1/2}g^{\kappa\alpha}_{m\mathbf{k},m'\mathbf{k}'}\varepsilon^{\kappa\alpha}_\lambda(\mathbf{k}-\mathbf{k}') , \tag{4}$$

$$g^{\kappa\alpha}_{l\mathbf{k},l'\mathbf{k}'}=\sum_{\beta_1 m_1,\beta_2 m_2}A^*(l\mathbf{k}|\beta_1 m_1)[\gamma_\alpha(\beta_1 m_1,\beta_2 m_2|\mathbf{k}')\delta_{\beta_1\kappa}-\gamma_\alpha(\beta_1 m_1,\beta_2 m_2|\mathbf{k})\delta_{\beta_2\kappa}+w_{\kappa,\alpha}(\beta_1 m_1\beta_2 m_2|\mathbf{k},\mathbf{k}')]A(l'\mathbf{k}'|\beta_2 m_2) . \tag{5}$$

In these equations, $\omega_\lambda(\mathbf{k})$ and $\varepsilon^{\kappa\alpha}_\lambda(\mathbf{k})$ are the frequency and eigenvector components for a phonon of wave vector ($\mathbf{k}$) and branch λ, M_κ is the mass of the κth atom, and $A(l\mathbf{k}|\beta m)$ is a component of the wave function for an electron in band l of wave vector $\mathbf{k}$. The notation βm refers to the mth component orbital of the basis (atomic) wave function on site $\beta[\varphi_{\beta m}]$. The γ's are given by

$$\gamma_\alpha(\beta_1 m_1,\beta_2 m_2|\mathbf{k})=\sum e^{-i\mathbf{k}\cdot\mathbf{R}_\sigma}\nabla_\alpha[H(\beta_1 m_1,\beta_2 m_2,\mathbf{R}_\sigma)-\varepsilon S(\beta_1 m_1,\beta_2 m_2,\mathbf{R}_\sigma)] , \tag{6}$$

in which H is a matrix element of the Hamiltonian on the localized basis,

$$H(\beta_1 m_1,\beta_2 m_2,\mathbf{R}_\sigma)=\int\varphi^*_{m_1}(\mathbf{r}-\mathbf{d}_{\beta_1}-\mathbf{R}_\sigma)H\varphi_{m_2}(\mathbf{r}-\mathbf{d}_{\beta_2})d^3r . \tag{7}$$

The derivative refers to the αth rectangular coordinate of the relative position vector of the two atoms,

$$\mathbf{X}=\mathbf{R}_\sigma+\mathbf{d}_{\beta_1}-\mathbf{d}_{\beta_2} ,$$

and d_β is the position of atom β relative to the local origin. The similar quantity S is an element of the overlap matrix [put $H=1$ in (7)] and

$$\varepsilon=\tfrac{1}{2}[E_l(\mathbf{k})+E_{l'}(\mathbf{k}')] .$$

Equation (5) has been written in a form in which the quantities γ_α of Eq. (6) contain only the change in the matrix elements of the Hamiltonian due to displacement of the orbital basis by a phonon. The third term in Eq. (5), w_α, contains the change in the atomic potentials produced by displacements of the ions:

$$w_{\kappa\alpha}(\beta_1 m_1,\beta_2 m_2|\mathbf{k},\mathbf{k}')=\sum_\sigma e^{-i\mathbf{k}\cdot\mathbf{R}_\sigma}\sum_\eta e^{i(\mathbf{k}-\mathbf{k}')\cdot\mathbf{R}_\eta}\int\varphi^*_{m_1}(\mathbf{r}-\mathbf{d}_{\beta_1}-\mathbf{R}_\sigma)[\nabla_\alpha V(\mathbf{r}-\mathbf{d}_\kappa-\mathbf{R}_\eta)]\varphi_{m_2}(\mathbf{r}-\mathbf{d}_{\beta_1})d^3r . \tag{8}$$

This term is implied in Ref. 13, but is not explicitly exhibited there.

In principle, there is no reason, other than computational complexity, why all these quantities should not be computed from first principles. This requires, for example, explicit differentiation of matrix elements with respect to atomic positions. In addition, evaluation of Eq. (8) would perhaps be even more complex than is apparent at first sight from the formula in that the gradient of the potential implicitly includes the effects of a self-consistent change in the electron distribution. In practice (and this applies to our calculation), Eq. (5) is not evaluated exactly. We list the approximations employed in our work below. We believe them to be reasonably standard and conventional in that they are included in NTB calculations of which we are aware.

(1) The potential terms in $w_{\kappa\alpha}$ which involve three centers are ignored.

(2) The quantities γ_α are found numerically in a rather indirect manner as follows. An orthogonal two-center tight-binding fit (Slater-Koster type[26]) is made to the calculated band structure. The lattice parameters are then changed (specifics are given in the next section); the band calculation and the tight-binding parametrization are repeated. The differences of the parameters from the tight-binding fits are used to determine the derivatives of the Hamiltonian matrix elements. This procedure enables one to include the two terms in Eq. (8) that occur in a two-center approximation. Since orthogonal tight-binding fits are used, the gradients of the overlap matrix in Eq. (6) are ignored. In our work, we have evaluated Eq. (5) using the wave functions [quantities $A(l\mathbf{k}|\beta_m)$] from the first-principles calculation, since this is what is required by the argument leading to Eq. (5). Some authors use the wave functions resulting from the Slater-Koster fit.

In view of the approximations involved in the use of the tight-binding fits, high accuracy cannot be claimed for the electron-phonon interaction parameters. Error in the range of 10–25% might be expected. However, there is considerable evidence that the procedure works rather well for many transition-metal compounds including such superconductors as Nb_3Sn.[13]

Equations (1) and (2) are not the most general forms of the Eliashberg equations because the pairing electron-phonon interaction has been restricted to states on the Fermi surface. We consider below in Sec. IV, in a very rough way, some possible consequences of the removal of this restriction.

The averaged quantities $\alpha^2F(\omega)$ and λ which are frequently considered are related to the coupling constants and frequencies by

$$\alpha^2F(\omega)=\frac{\Omega}{(2\pi)^3}\sum_{mm'}\int\frac{dS_\mathbf{k}}{|\nabla_\mathbf{k}E_{m\mathbf{k}}|}\int\frac{dS_{\mathbf{k}'}}{|\nabla_{\mathbf{k}'}E_{m'\mathbf{k}'}|}\sum_\lambda|g_{m'\mathbf{k}'m\mathbf{k}\lambda}|^2\delta(\omega-\omega_\lambda(\mathbf{k}'-\mathbf{k}))\Big/\sum_m\int\frac{dS_\mathbf{k}}{|\nabla_\mathbf{k}E_{m\mathbf{k}}|} , \tag{9}$$

and

$$\lambda = 2\int_0^\infty \alpha^2 F(\omega) d\omega/\omega \ . \tag{10}$$

In order to determine the gap function Δ at $T=0$, we use the anisotropic Eliashberg equations for real frequencies as given by Carbotte[27]

$$\Delta_m(\mathbf{k},\omega)Z_m(\mathbf{k},\omega) = \int_0^{\omega_c} d\omega' \sum_{m'} \frac{\Omega}{(2\pi)^3} \int \frac{dS_{\mathbf{k}'}}{|\nabla_{\mathbf{k}'} E_{m\mathbf{k}'}|} \mathrm{Re}\left\{ \frac{\Delta_{m'}(\mathbf{k}',\omega')}{\sqrt{\omega'^2 - \Delta^2_{m'}(\mathbf{k}',\omega')}} \right\} \times \left[\int_0^\infty d\nu \sum_\lambda |g_{m\mathbf{k},m'\mathbf{k}',\lambda}|^2 \delta(\nu - \omega_\lambda(\mathbf{k}'-\mathbf{k})) K_+(\omega,\omega',\nu) - U_c \right] , \tag{11}$$

and

$$[1 - Z_m(\mathbf{k},\omega)]\omega = \int_0^{\omega_c} d\omega' \frac{\Omega}{(2\pi)^3} \sum_{m'} \int \frac{dS_{\mathbf{k}'}}{|\nabla_{\mathbf{k}'} E_{m'\mathbf{k}'}|} \mathrm{Re}\left\{ \frac{\omega'}{\sqrt{\omega'^2 - \Delta^2_{m'}(\mathbf{k}',\omega')}} \right\} \times \left[\int_0^\infty d\nu \sum_\lambda |g_{m\mathbf{k},m'\mathbf{k}',\lambda}|^2 \delta(\nu - \omega_\lambda(\mathbf{k}'-\mathbf{k})) K_-(\omega,\omega',\nu) \right] , \tag{12}$$

in which

$$K_\pm(\omega,\omega',\nu) = \frac{1}{\omega'+\omega+\nu+i0^+} \pm \frac{1}{\omega'-\omega+\nu-i0^+} \ . \tag{13}$$

III. COMPUTATIONAL PROCEDURES AND PARAMETERS

A. Electronic structure

The first step was the calculation of the electronic structure (energy bands and wave functions) by the self-consistent LCAO method mentioned in the Introduction. The lattice parameters and atomic coordinates are those determined by Beno *et al.*,[28] and (after conversion to atomic units) are listed in Table I.

Atomic wave functions are used as basis functions in the solid-state calculation. The atomic functions were generated by a separate, self-consistent calculation employing an even-tempered basis of Gaussian orbitals. The basis set is specified by listing the number of terms, and the smallest and largest exponents for each element. This information is presented in Table II.

The procedure we employ for the calculation of the electron-phonon interaction requires, in one step, a Slater-Koster tight-binding fit to the calculated band structure.[26] In order to keep the number of parameters manageable, the basis set used in the band calculation was kept at a minimum size of 47. The atomic wave functions included were Y($5s,4d$), Ba($6s$), Cu($4s,3d$), and O($2p$). The atomic states of lower energy were treated as core states.

A grid of 72 points in the irreducible portion ($\frac{1}{8}$th) of the Brillouin zone (an odd $6\times6\times2$ mesh with unit weight for each point) was used in the self-consistent calculation. The total energy changed by only 0.004 Ry/cell when we increased the total number of k points considered from 18 to 72. The resulting band structure is shown in Fig. 1 of Ref. 1, in which the origin of the energy scale has been shifted to the Fermi energy. This band structure agrees well with other recent calculations.[17]

The first-principles band structure was then fitted by an orthogonal Slater-Koster tight-binding procedure.[26] The fit was based on energies at 18 points in the zone of relatively high symmetry. The band structure of $YBa_2Cu_3O_7$ does not show degeneracies at any $\mathbf{k}$ points, which removes one of the features usually employed to determine symmetries of levels. However, the wave functions still have some useful symmetries at some $\mathbf{k}$ points

TABLE I. Lattice parameters (in bohrs) and atomic coordinates. $a=7.2446$, $b=7.3442$, $c=22.0733$.

	x/a	y/b	Z/c
y	$\frac{1}{2}$	$\frac{1}{2}$	$\frac{1}{2}$
Ba	$\frac{1}{2}$	$\frac{1}{2}$	0.1843
	$\frac{1}{2}$	$\frac{1}{2}$	−0.1843
Cu(1) chain	0	0	0
Cu(2) plane	0	0	0.3556
	0	0	−0.3556
O(1) chain	0	$\frac{1}{2}$	0
O(2) plane	$\frac{1}{2}$	0	0.3773
	$\frac{1}{2}$	0	−0.3773
O(3) plane	0	$\frac{1}{2}$	0.3789
	0	$\frac{1}{2}$	−0.3789
O(4) apical	0	0	0.1584
	0	0	−0.1584

TABLE II. Gaussian basis set atomic functions: N_s, N_p, N_d are the number of terms of s,p,d type, $\alpha_{\min}$ the smallest orbital exponent, $\alpha_{\max}$ the largest orbital exponent. The d functions have the same smallest exponent and same ratio of successive exponents as for s and p functions, but the maximum exponent is smaller.

Atom	N_s	N_p	N_d	$\alpha_{\min}$	$\alpha_{\max}$
Y	17	17	14	0.318 186	$0.224\,97\times10^7$
Ba	19	19	16	0.173 904	$0.361\,98\times10^6$
Cu	17	17	14	0.357 135	$0.140\,54\times10^7$
O	18	18		0.471 188	0.10×10^7

of high symmetry. Group theory was used to determine these symmetries so that irreducible representations could be fitted separately. In the first stage of the fitting, all bands were included and an average (rms) error of about 12 meV was attained. Then the energy bands around E_f were assigned higher weights since these are the most important for the electron-phonon interaction. The average error was reduced to 9 meV, while the fitting errors for the bands close to E_f are only about 5 meV.

The distances between the pairs of neighbors that were included in the tight-binding parametrization are given in Table III. The parameters as determined from the fit are given in Tables IV(a), IV(b), IV(c), and IV(d). There are a total of 114 tight-binding parameters. In Table IV, TB (Ry) is the tight-binding parameter; DTB=$dt(r)/dr$ is the radial derivative of the tight-binding parameter $t(r)$ in Ry/a.u.; CF means the crystal-field parameter. The gradients of the on-site parameters were chosen as zero. We believe these parameters give a good description of the electronic structure of YBCO, but there are still some residual errors. We used the tight-binding fit only to extract derivatives of the Hamiltonian with respect to atomic displacements.

B. Lattice vibrations

Although the theory of lattice dynamics and the electron-phonon interaction employed in this paper[13] yields predictions for the phonon spectrum, we considered it to be preferable to use phonon frequencies and eigenvectors that might be closer to experiment. We obtained these quantities from a shell-model calculation using parameters determined by Humlicek *et al.*[25] from a fit to the observed Raman and infrared spectra. The calculated frequencies for the Raman-active phonons agree well with experimental measurements as shown in Fig. 10 of Ref. 25. The phonon dispersion curves are shown in Figs. 1(a), 1(b), and 1(c), where they are compared with results of neutron scattering measurements reported by Reichardt *et al.*[29] The agreement seems to be reasonably good. We have not included any renormalization of the phonon frequencies due to electron-phonon interactions not included in the shell model. Since we find strong interactions with phonons of about 65 meV energy, it is possible that some contribution of this type should be included, particularly for large q.

C. Electron-phonon interaction

The electron-phonon interaction was calculated according to the procedures described in Ref. 13. According to Eqs. (5) and (6), we require gradients of matrix elements of the Hamiltonian with respect to atomic displacements. In order to obtain these, the first-principles band calculation was repeated with the lattice parameters reduced by 2%. The tight-binding fit was also repeated. The dependence on separation distance of the tight-binding parameters involving orbitals on different sites was assumed to be of the form $e^{\alpha d}$, where d is the distance between sites. The determination of derivatives of the Hamiltonian is only accurate to about 10–25 %. Additional ionic contributions to the electron-phonon in-

TABLE III. The pair distances in orthorhombic $YBa_2Cu_3O_7$ (in a.u.).

			First neighbors					
Atom/Atom	Y	Ba	Cu(1)	Cu(2)	O(1)	O(2)	O(3)	O(4)
Y				6.0574		4.5629	4.4938	
Ba			6.5637	6.3899	5.4404	5.6244	5.6125	5.1827
Cu(1)		6.5637	7.2246		3.6721			3.4964
Cu(2)	6.0574	6.3899		6.3748		3.6440	3.7080	4.3529
O(1)		5.4404	3.6721		7.2246			5.0704
O(2)	4.5629	5.6244		3.6440		5.4168	5.1512	6.0329
O(3)	4.4938	5.6125		3.7080		5.1512	5.3462	6.0970
O(4)		5.1827	3.4964	4.3529	5.0704	6.0329	6.0970	6.9928

			Second neighbors			
Atom/Atom	Cu(1)	Cu(2)	O(1)	O(2)	O(3)	O(4)
Cu(1)	7.3442					
Cu(2)		7.2246		6.9144	6.9159	
O(1)			7.3442			
O(2)		6.9144		7.2246	7.4494	
O(3)		6.9159		7.4494	7.2246	
O(4)						7.2246

			Third neighbors	
Atom/Atom	Cu(2)	O(2)	O(3)	O(4)
Cu(2)	7.3442			
O(2)		7.3442		
O(3)			7.3442	
O(4)				7.3442

TABLE IV. The tight-binding parameters for orthorhombic $YBa_2Cu_3O_7$ (in Ry). Here CF means the crystal-field parameter; TB is the tight-binding parameter in Ry; DTB is the radial derivative of TB in Ry/a.u.

(a) On-site parameters

Atom	E_s	E_p	E_d	CF ($dd\sigma$)	CF ($sd\sigma$)
Y	0.7122		0.2233	0.0320	−0.0337
Ba	0.3948				
Cu(1)	0.3221		−0.4183	0.0465	0.0619
Cu(2)	0.4173		−0.3921	0.0108	0.0281
O(1)		−0.0595			
O(2)		−0.0470			
O(3)		−0.0626			
O(4)		−0.0771			

(b) First neighbors

Pair		TB (Ry)	DTB (Ry/a.u.)	Pair		TB (Ry)	DTB (Ry/a.u.)
Y-Cu(2)	$ss\sigma$	0.0852	0.127	Cu(2)-Cu(2)	$ss\sigma$	0.0244	0.015
	$sd\sigma$	0.0026	−0.028		$sd\sigma$	−0.0246	0.089
	$dd\sigma$	0.0599	−0.209		$dd\sigma$	−0.0057	0.053
	$dd\pi$	0.0101	−0.047		$dd\pi$	0.0059	0.029
	$dd\delta$	−0.0161	0.053		$dd\delta$	0.0072	0.064
Y-O(2)	$sp\sigma$	0.0472	0.236	Cu(2)-O(2)	$sp\sigma$	0.2006	−0.310
	$dp\sigma$	0.1669	−0.045		$dp\sigma$	−0.1188	0.113
	$dp\pi$	−0.0496	0.139		$dp\pi$	0.0616	0.190
Y-O(3)	$sp\sigma$	0.0433	0.314	Cu(2)-O(3)	$sp\sigma$	0.2002	−0.188
	$dp\sigma$	0.1675	−0.124		$dp\sigma$	−0.1107	0.154
	$dp\pi$	−0.0561	0.138		$dp\pi$	0.0544	0.264
Ba-Cu(1)	$ss\sigma$	−0.0055	0.034	Cu(1)-O(4)	$sp\sigma$	0.1329	−0.046
	$sd\sigma$	−0.0806	0.036		$dp\sigma$	−0.0796	−0.222
Ba-Cu(2)	$ss\sigma$	0.0634	0.039		$dp\pi$	0.0192	0.027
	$sd\sigma$	−0.0622	0.083	O(1)-O(1)	$pp\sigma$	−0.0386	0.074
Ba-O(1)	$sp\sigma$	−0.0965	0.261		$pp\pi$	−0.0138	−0.008
Ba-O(2)	$sp\sigma$	−0.0573	0.057	O(1)-O(4)	$pp\sigma$	−0.0027	0.026
Ba-O(3)	$sp\sigma$	−0.0410	0.085		$pp\pi$	0.0054	−0.032
Ba-O(4)	$sp\sigma$	−0.1002	0.114	O(2)-O(2)	$pp\sigma$	0.0135	0.088
Cu(1)-Cu(1)	$ss\sigma$	−0.0286	0.015		$pp\pi$	−0.0047	−0.004
	$sd\sigma$	0.0132	0.102	O(2)-O(3)	$pp\sigma$	0.0189	0.023
	$dd\sigma$	0.0094	−0.012		$pp\pi$	−0.0030	−0.016
	$dd\pi$	−0.0107	0.089	O(2)-O(4)	$pp\sigma$	−0.0082	−0.018
	$dd\delta$	0.0062	0.000		$pp\pi$	−0.0081	−0.016
Cu(1)-O(1)	$sp\sigma$	0.2620	−0.167	O(3)-O(3)	$pp\sigma$	−0.0139	0.061
	$dp\sigma$	−0.0894	0.071		$pp\pi$	0.0085	−0.022
	$dp\pi$	−0.0073	0.125	O(3)-O(4)	$pp\sigma$	−0.0004	−0.002
Cu(1)-O(4)	$sp\sigma$	0.2153	−0.391		$pp\pi$	−0.0065	−0.001
	$dp\sigma$	−0.2090	0.105	O(4)-O(4)	$pp\sigma$	−0.0158	0.041
	$dp\pi$	0.0767	0.386		$pp\pi$	−0.0377	0.058

(c) Second neighbors

Pair		TB (Ry)	DTB (Ry/a.u.)	Pair		TB (Ry)	DTB (Ry/a.u.)
Cu(1)-Cu(1)	$ss\sigma$	−0.0430	−0.212	O(1)-O(1)	$pp\sigma$	0.0009	0.005
	$sd\sigma$	−0.0325	−0.111		$pp\pi$	−0.0039	−0.019
	$dd\sigma$	0.0061	0.031	O(2)-O(2)	$pp\sigma$	−0.0203	0.041
	$dd\pi$	−0.0031	0.029		$pp\pi$	0.0020	0.010
	$dd\delta$	0.0033	−0.041	O(2)-O(3)	$pp\sigma$	0.0126	−0.021
Cu(2)-Cu(2)	$ss\sigma$	−0.0061	−0.031		$pp\pi$	−0.0124	0.021
	$sd\sigma$	−0.0092	0.024	O(3)-O(3)	$pp\sigma$	−0.0072	−0.009
	$dd\sigma$	0.0003	0.002		$pp\pi$	−0.0056	−0.013
	$dd\pi$	0.0046	−0.038	O(4)-O(4)	$pp\sigma$	−0.0081	0.016
	$dd\delta$	0.0020	−0.011		$pp\pi$	0.0011	−0.003
Cu(2)-O(2)	$sp\sigma$	−0.0222	0.083	Cu(2)-Cu(3)	$sp\sigma$	−0.0066	−0.032
	$dp\sigma$	0.0031	−0.009		$dp\sigma$	0.0396	−0.089
	$dp\pi$	0.0150	−0.018		$dp\pi$	0.0238	0.043

TABLE IV. (*Continued*).

				(d) Third neighbors			
Pair		TB (Ry)	DTB (Ry/a.u.)	Pair		TB (Ry)	DTB (Ry/a.u.)
Cu(2)-Cu(2)	$ss\sigma$	−0.0126	−0.122	O(3)-O(3)	$pp\sigma$	−0.0053	0.020
	$sd\sigma$	−0.0113	0.003		$pp\pi$	−0.0011	0.010
	$dd\sigma$	0.0057	−0.034	O(4)-O(4)	$pp\sigma$	−0.0099	0.013
	$dd\pi$	−0.0010	0.009		$pp\pi$	−0.0004	0.002
	$dd\delta$	−0.0031	0.005				
O(2)-O(2)	$pp\sigma$	0.0043	0.015				
	$pp\pi$	−0.0032	−0.028				

teraction were not included.[30–32] From our calculation, it is found that the narrow-band structures around the Fermi energy give the most important contribution to the *e*-ph interaction in YBCO.

There is an ambiguity about orthonormality which arises in the sequence of approximations involved in the evaluation of Eq. (5). The wave functions A in the first-principles calculation obey $\langle A|S|A\rangle = I$ where I is a unit matrix and S is the overlap matrix. On the other hand, in a two-center orthogonal tight-binding approach, the wave functions (which we denote by U) satisfy $\langle U|U\rangle = I$. We have checked that this difference is not a significant one for the narrow-band electronic states near the Fermi energy by calculating $\langle A|A\rangle$. We found that the diagonal elements of $\langle A|A\rangle$ were in the range 1.02–1.04 and that the off-diagonal elements were of the order 10^{-6}. However, this does not imply that the same results for the interaction constants g will be obtained if U is used in place of A in Eq. (5). Ideally, U and A would be related by the transformation $U = S^{1/2}A$. This is not the case, however, in the actual calculation. Although the energies, particularly for states near E_f, from the tight-binding fit are matched as closely as possible to the energies from the first-principles calculation, no detailed attempt is made to relate the wave functions, except that symmetry types (irreducible representations) are required to correspond. The differences between the wave functions are not simply described by an overall normalization factor. Since the overall normalization problem is not serious near E_f, we think that use of A in Eq. (5) is reasonable, even when the gradients [Eq. (6)] are obtained from a fit, rather than a full calculation. We emphasize that we employ the fit only in the evaluation of Eq. (6).

D. Solution of the Eliashberg equations

The evaluation of the k-dependent quantities employed twin grids: 845 **k** points on an even mesh and 576 k points on an odd mesh. Both numbers refer to the entire Brillouin zone. Each **k** point on the odd mesh is the center of a little cube, and is surrounded by eight **k** points of the even mesh on the corners. The matrix elements were calculated for the **k** points of the odd mesh, while the contribution to the density of states from the little cube was found based on the even-mesh **k** points by the tetrahedral method.

Symmetry was used to simplify the solution of the anisotropic gap equations. The electron-phonon interaction does not break the full crystal symmetry of the gap function (this point was checked carefully). Hence it is possible to compute the gap function only within the irreducible Brillouin zone, while scattering processes over the entire zone were considered.

T_c was determined from Eqs. (1) and (2) by matrix diagonalization as discussed by Allen and Mitrovic.[2] The maximum value of n' in the summations of Eqs. (1) and (2) was taken as $n' = N = 20$. The results do not change appreciably for $N > 15$, indicating convergence.

The gap equations for $T = 0$, Eqs. (11) and (12), were considered in a four-dimensional form and solved by iteration using the same **k**-point mesh as in the calculation of T_c. A cutoff frequency ω_c of 800 meV was used. The frequency integrations were performed on a grid of 1500 evenly spaced points (step size 0.53 meV). The small positive number 0^+ in the expression (11) for $K_\pm$ was chosen to be $\frac{1}{5}$th of the step size (0.106 meV). As a convergence criterion, we required that the average difference of two consecutive solutions should be less than 0.13 meV. The solutions differed by about 0.2 meV when the number of integration steps was increased from 1000 to 1500. We believe this indicates satisfactory con-

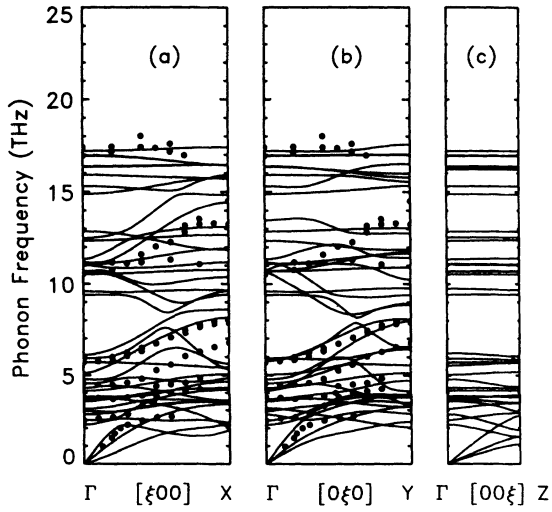

FIG. 1. Calculated phonon dispersion curves using a shell model for orthorhombic $YBa_2Cu_3O_7$ along Γ-X (a), Γ-Y (b), and Γ-Z (c) directions. The dots are experimental results of Ref. 29.

vergence and stability in regard to the energy grid.

It was possible to test portions of the computer program for Nb. A separate band calculation was made to generate wave functions, but the tight-binding parameters were obtained from the literature.[13] A force-constant model was used for the phonons. Good agreement was found in comparison with published results.[13]

IV. RESULTS: T_c

The calculated value of λ was about 1.95 and the density of states was 2.45 states/eV cell spin. Reference 17 reports a calculated λ of 1.7 based on a much smaller sample of the phonon spectrum. We think the agreement is reasonable. Our calculated T_c is about 90.5 K for $\mu^*=0.1$ and 94 K for $\mu^*=0$. The excellent agreement between the calculation and observation is both surprising and pleasing, but must be regarded as somewhat fortuitous since the calculation of derivatives of the Hamiltonian matrix probably is accurate only within 10–25 %. However, it is evident that the electron-phonon interaction can lead to a high T_c in this material, contrary to the conclusion of Ref. 11. We note that the authors of Ref. 29 interpreted some features of their measurements of the phonon dispersion curves in YBCO as indicating the presence of a strong electron interaction with high-frequency phonons. It remains, however, to be determined whether a λ of the size we find here is consistent with the transport properties in the normal state.

We believe our results indicate the importance of performing a complete calculation treating the electronic structure and the phonon spectrum in detail. If one uses instead of the **k**-dependent equations, Eqs. (1) and (2), the averaged, energy-dependent isotropic Eliashberg equations, then T_c is found to be about 83 K for $\mu^*=0.0$ and 63 K for $\mu^*=0.1$. The values are significantly inferior. We have discussed above, in Sec. III C, the possible use of wave functions from the tight-binding fit (U) rather than those from the first-principles calculation in the calculation electron-phonon interaction according to Eq. (5). If this substitution is made, we find $T_c=67$ K for $\mu^*=0$. If, in addition, the energy bands from the fit are used in the solution of the Eliashberg equations (1) and (2), T_c is further reduced to about 40 K, much closer to the results of Ref. 11. Residual inaccuracies in the tight-binding fit are probably responsible for the additional difference. The density of states at E_f calculated from the fit is only 0.64 of that obtained from the first-principles calculation.

The phonon density of states and the isotropic coupling function $\alpha^2F(\omega)$ are shown in Fig. 2 of Ref. 1. It will be seen that we have strong coupling with optical phonons in the energy range 60–73 meV. In this respect, our result contrasts strongly with that of Ref. 11. This energy range strongly involves oxygen motions, in particular, the apical and planar oxygens [O(2),O(3),O(4)]. Our value of T_c is roughly consistent with the observation of Carbotte,[3] mentioned in the Introduction, that under conditions of strong coupling to phonons in a narrow range, T_c could be as much as $\frac{2}{15}$ of a typical phonon frequency ω_0. The ω_0 corresponding in this way to $T_c\approx 90$ K is 58 meV.

We have made several calculations to determine how sensitive is the calculated T_c to the position of the Fermi energy, and therefore to the detailed band structure of the electronic states. If E_f is lowered by 0.03 eV, T_c changes only by a relatively small amount ($T_c\sim 85$ K). However, substantial further lowering puts E_f in the flat-band complex. Both the density of states and T_c rise markedly. (We do not imply that the density of states determines T_c directly.) Reducing E_f by 0.09 eV increases the density of states to 8.0 states/eV cell spin, and T_c rises to about 165 K. A similar increase from $T_c=67$ K to $T_c=110$ K occurs if the tight-binding wave functions U are used and E_f is lowered. On the other hand, if E_f is raised, the flatbands are occupied, and the density of states and T_c both decrease. For example, if E_f is raised by 0.02 eV, the density of states is reduced to 1.6 states/eV cell spin, and T_c is about 50 K. It should be noted that this reduction of T_c as E_f increases is consistent with the observed behavior of T_c in YBCO as the oxygen content is reduced. These results suggest that the narrow bands around the Fermi energy make a very important contribution to the e-ph interaction. The superconductivity of YBCO cannot be understood if the narrow bands near E_f are neglected.

A major objection to the acceptance of the electron-phonon interaction as the source of the observed high T_cs in YBCO is the smallness of the isotope effect, mentioned above in the Introduction. This is a serious problem for us because this calculation requires a rather strong interaction between the electrons and the high-frequency oxygen phonons. We investigated the isotope effect by repeating the calculation of T_c keeping all parameters the same except for a change in the mass of some (or all) oxygen from 16 to 18. When the masses of the chain [O(1)] and plane oxygens [O(2) and O(3)] were changed from ^{16}O to ^{18}O, T_c remained the same. However, changing the mass of the apical oxygens [O(4)] produced a shift in T_c by about -3 K.

A small isotope shift in T_c, -0.18 ± 0.02 K, is observed experimentally when all oxygen sites are changed from ^{16}O to ^{18}O. A recent experiment measured the oxygen isotope shift when specific types of sites are changed from ^{16}O to ^{18}O.[33] It was found that, if the plane oxygens are changed from ^{16}O to ^{18}O, a small increase in T_c (negative isotope effect) results, in contrast to the small decrease observed when all sites are equally substituted. Our results for plane substitution are at least partly consistent with this experiment, but the change resulting from substituting the apical oxygen is clearly too large. The effect of the inclusion of other possible interactions on T_c and on the isotope effect remains to be investigated.

Also, we speculate that another effect may need to be considered. The electronic states at **k** and **k**′ in Eqs. (1) and (2) are restricted to the Fermi surface. This is a good approximation for simple metals since the conduction band is much wider than any phonon energy. In YBCO, however, the optical phonon energies (up to 80 meV) are not small, compared to the energy scale on which the band structure varies significantly. The narrow bands

close to E_f can make a very significant contribution to the interaction. Transitions are possible between states which are within a phonon energy of the Fermi energy. We can simulate this roughly by replacing the δ function in Eqs. (1) and (2) by

$$\delta(\varepsilon)=\begin{cases}1/2d & \text{for } |\varepsilon|<d\ ,\\ 0 & \text{otherwise}\ .\end{cases} \tag{14}$$

Here we used $d=\omega_m\sqrt{(16/M_0)}$; $\omega_m=0.08$ eV; M_0 is the mass of the oxygen atom in atomic units. Then we evaluated the shift of T_c due to the isotope effect of the oxygen atoms. We repeated the calculations using the mass of all oxygen atoms as 16 and 18, respectively, and calculated the T_c value from Eqs. (1) and (2) and using Eq. (14). It is found that, when the Fermi energy is such that T_c is in the range from 85 to 93 K, the T_c shift is almost zero when the oxygen mass is changed from 16 to 18. When the Fermi energy is raised to well above the narrow bands, then T_c is found to be at about 50–60 K and the oxygen isotope effect becomes large as in the conventional superconductors. This is because the density of states is flat and the smearing has little effect.

V. RESULTS: THE GAP FUNCTION

The calculated energy gaps at $T=0$ K and the Fermi surface are shown in Fig. 2. In Fig. 2, the energy gaps in the dark shaded regions have values in the range $18<\Delta_0<25$ meV; the light shaded regions have the energy-gap values of $12.2<\Delta_0<14$ meV; all other regions have smaller energy gaps in the range $10<\Delta_0<12.2$ meV. We divided the Brillouin zone into little cubes and the energy gap in each little cube is treated as constant in our calculation. This leads to a discontinuity of the marked values on the boundary of two regions. The Fermi energy E_f is very near the top of some bands as seen from Fig. 1 of Ref. 1. The energy gaps do not change much along the k_z direction, a property which we associate with the approximate two-dimensional nature of this system. The only significant exception to this is that the gap in the region marked 1 in Fig. 2 varies from about 24 meV for $k_z=0$ to 18 meV for $k_z=\pi/c$.

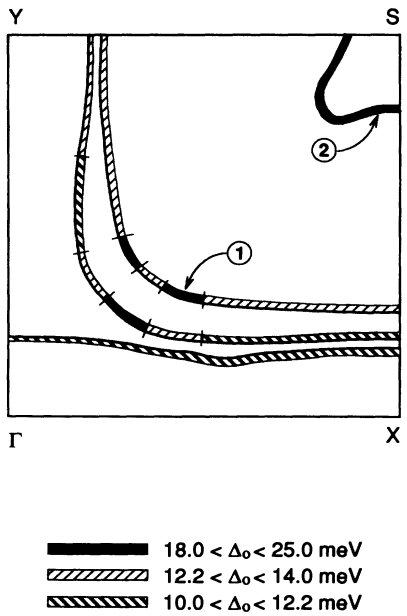

FIG. 2. Superconducting energy gap on the Fermi surface of orthorhombic $YBa_2Cu_3O_7$ at $T=0$ K. The dark shaded region: $18<\Delta_0<25$ meV; lightly hatched region: $12.2<\Delta_0<14$ meV; dark hatched: $10<\Delta_0<12.2$ meV.

The gap function has a strong variation with k, and also a strong variation between different sheets of the Fermi surface. A **k**-dependent gap function has previously been derived by Mahan[34] under the assumption of dominant electron-phonon coupling. However, he considered only a two-dimensional, one-band model. As was mentioned above, in Sec. II, the gap function should be considered as a vector with components in the different bands which cross the Fermi surface, $\Delta_n(\mathbf{k})$, rather than as a single function. Here we find a substantial variation between the different components. From inspection of Fig. 2, it can be seen that the energy gap is quite large on the small piece of Fermi surface around the S point, ranging from about 18 to 24 meV ($2\Delta/k_BT_c$ varies from 4.4 to 6.0). The gap value tends to be significantly smaller on the large sheets of the Fermi surface, although there are small portions where it is quite large. Proceeding outward from the small piece of the Fermi surface at the S point, the gap on most of the next two large sheets of the Fermi surface is in the range of 11–14 meV, but there are small regions near the Γ-S line where the gap value is much larger. The two portions of the Fermi surface which have the largest gap values are marked 1 and 2. The gap on the outermost sheet (from a chain $pd\sigma$ band) has the value in the range 10–12 meV. In terms of $2\Delta/k_BT_c$, the total range over the Fermi surface is from 2.5 to 6.0. Many experimental results, based on Raman spectroscopy,[35] tunneling,[36] and nuclear magnetic resonance,[37] are in this range. A few examples are contained in the references cited above. However, it may be necessary to reconsider the interpretation of some experiments if the strong **k** and band dependence of the gap we predict here is correct.

Both the calculation of T_c and that of the gap function involve the narrow bands near E_f in an important way. At the zone edge (point S), one of these bands is just above E_f, giving rise to a small piece of Fermi surface with a large gap, shown in Fig. 2. The other band is slightly below E_f there. If E_f is raised to be above both bands, T_c decreases substantially; if it is lowered so that the lower band participates, T_c increases. Examination of the wave function show that, in both cases, the largest components are associated with functions of p_x and p_y symmetry on the apex oxygens [O(4)] which hybridize with d_{yz} and d_{zx} functions on the chain copper [Cu(1)]. Consideration of the shapes of these orbitals suggests that the orbital overlap and interaction would be sensitive to the c axis motion of the O(4). This is consistent with the importance of O(4) vibrations in our calculation, mentioned above.

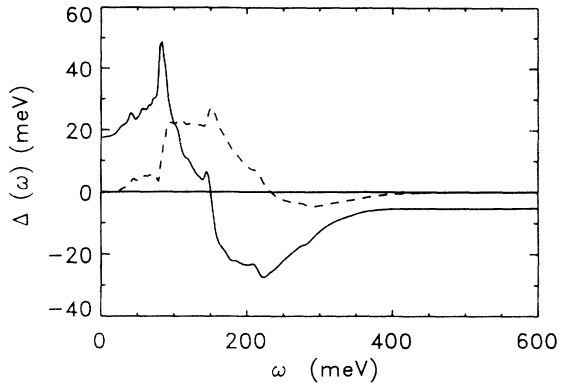

FIG. 3. Average isotropic energy gap function $\Delta(\omega)$. $\mu^*=0.1$. Solid line: the real part of $\Delta(\omega)$; dashed line: the imaginary part of $\Delta(\omega)$.

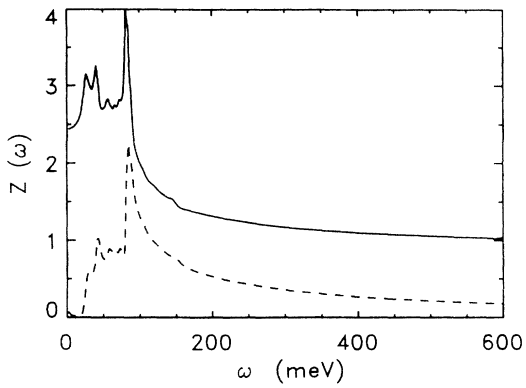

FIG. 4. Average isotropic renormalization function $Z(\omega)$. Solid line: the real part of $Z(\omega)$; dashed line: the imaginary part of $Z(\omega)$.

In Fig. 3, we have shown the real and imaginary parts of the **k**-space average of the gap function $\Delta(\omega)$ at $T=0$. The similarly averaged renormalization function $Z(\omega)$ is shown in Fig. 4. The general shapes of these curves are similar to what has been obtained in low-temperature superconductors,[38] except that both the magnitudes of these functions and the range of frequency variation are much larger in the present case. Unfortunately, it may not be possible to use these **k**-averaged frequency-dependent quantities directly. For example, it will be necessary to consider the **k** and band dependence explicitly in the calculation of the density of quasiparticle states.

VI. CONCLUDING DISCUSSION

We believe these calculations make a strong case that consideration of the electron-phonon interaction is essential to understanding superconductivity in YBCO. Our very detailed calculations lead to a T_c close to the experimental value. It is possible that phonon interactions along are sufficient, but it is also possible that other interactions extensively discussed in the literature may play some role. It remains also to be investigated whether the strong electron interaction with optical phonons that we find here is consistent with transport properties in the normal state. A full theory still appears to be rather distant.

All local-density band calculations predict that the Fermi surface of YBCO has four sheets. We find that there is a substantial variation of the gap function between the different sheets as well as a positional variation on a given sheet. We think it possible that such behavior will occur whatever interactions are important. If this is correct, there are profound consequences for the interpretation of measurements of many aspects of the superconducting state; tunneling being only the most obvious. One-band models are probably quite inadequate in YBCO, although of course there may be other cuprates ($Nd_{2-x}Cd_xCuO_4$ is an example) where a single-band description may be satisfactory. But in YBCO even some of the narrow bands near E_f appear to be important.

The smallness of the isotope effect in YBCO has generally been interpreted as implying that phonons are not importantly involved in its superconductivity. If YBCO were a metal with simple crystallographic and electronic structures, this conclusion would probably be correct. But the study of the isotope effect in YBCO involves much more than just the phonon energies. The details of the electron-phonon interaction have to be considered. There are other questions, such as the possible role of lattice anharmonicity. We believe that it is reasonable at this time to search for a possible solution to the isotope effect problem within the framework of a dominant electron-phonon interaction. One way in which a solution might be found, involving consideration of transitions between states close to, but not precisely on, the Fermi surface, was sketched roughly in the text.

Some readers may object to our reliance on the electronic structure calculated in the local-density approximation for the study of the electron-phonon interaction, from the view that if short-range repulsive electron-electron interactions (a Hubbard U) were more adequately included, the strength of the electron-phonon coupling would be reduced.[39] However, we do not believe that a simple one- or even three-band model in which short-range contributions to the electron interaction alone are included is adequate for such considerations. We speculate that, if a more realistic model of the band structure of $YBa_2Cu_3O_7$ is considered, the presence of low-energy resonant structure in the dielectric function[40] may contribute to the pairing interaction either directly, or by enhancement of the electron-phonon interaction.

ACKNOWLEDGMENTS

We are grateful to A. Omeltchenko and to Dr. Han Chen for providing us with, and helping us to use, a program for the phonon spectrum calculations on the basis of the shell model. This research was supported in part by the National Science Foundation under Grant No. DMR 91-20166.

[1]G. L. Zhao and J. Callaway, Phys. Rev. B **49**, 6424 (1994).
[2]P. B. Allen and B. Mitrovic, in *Solid State Physics: Advances in Research and Applications,* edited by H. Ehrenreich and D. Turnbull (Adademic, Orlando, 1982), Vol. 37, p. 1.
[3]J. P. Carbotte, Rev. Mod. Phys. **62**, 1027 (1990).
[4]M. Gurvitch and A. T. Fiory, Phys. Rev. Lett. **59**, 1337 (1987). A contrasting view is expressed by R. Zeyher, Phys. Rev. B **44**, 10 404 (1991).
[5]The still somewhat confused experimental situation in regard to the isotope effect in YBCO was summarized by J. P. Carbotte and E. J. Nicol, in *Lattice Effects in High-T_c Superconductors,* edited by Y. Bar Yam, T. Egami, J. Mustre-de Leon, and A. R. Bishop (World Scientific, Singapore, 1992), p. 189. These authors conclude that the isotope effect exponent β is about 0.05 in pure, stoichiometric $YBa_2Cu_3O_7$.
[6]T. W. Barbee III, M. L. Cohen, and D. R. Penn, Phys. Rev. B **44**, 4473 (1991).
[7]V. H. Crespi and M. H. Cohen, Phys. Rev. B **48**, 398 (1993).
[8]L. E. Rehn, R. P. Sharma, and P. M. Baldo, in *Lattice Effects in High-T_c Superconductors* (Ref. 5), p. 27.
[9]C. Thomsen, M. Cardona, B. Gegenheimer, R. Liu, and A. Simon, Phys. Rev. B **37**, 9860 (1988).
[10]J. M. Valles, Jr., R. C. Dynes, A. M. Cucolo, M. Gurvitch, L. F. Schneemeyer, J. P. Garno, and J. V. Waszczak, Phys. Rev. B **44**, 11 986 (1991).
[11]W. Weber and L. F. Mattheiss, Phys. Rev. B **37**, 599 (1988).
[12]L. F. Mattheiss and D. R. Hamann, Solid State Commun. **63**, 395 (1987).
[13]C. M. Varma and W. Weber, Phys. Rev. Lett. **39**, 1094 (1977); C. Varma, E. I. Blount, P. Vashishta, and W. Weber, Phys. Rev. B **19**, 6130 (1979); W. Weber, in *Electronic Structure of Complex Systems,* Vol. 113 of *NATO Advanced Study Institute, Series B: Physics,* edited by P. Phariseau and W. Temmerman (Plenum, New York, 1994), p. 345.
[14]W. E. Pickett, H. Krakauer, R. E. Cohen, and D. J. Singh, Science **255**, 46 (1992).
[15]W. Kress, U. Schröder, J. Prade, A. D. Kulkarni, and F. W. deWette, Phys. Rev. B **38**, 2906 (1988).
[16]R. E. Cohen, W. E. Pickett, and H. Krakauer, Phys. Rev. Lett. **64**, 2575 (1990).
[17]I. I. Mazin, O. K. Andersen, A. I. Liechtenstein, O. Jepsen, V. P. Antropov, S. N. Rashkeev, V. I. Anisimov, J. Zaanen, C. O. Rodriguez, and M. Methfessel, in *Lattice Effects in High-T_c Superconductors* (Ref. 5), p. 235.
[18]P. J. Feibelman, J. A. Appelbaum, and D. A. Hamann, Phys. Rev. B **20**, 1433 (1979).
[19]B. N. Harmon, W. Weber, and D. R. Hamann, Phys. Rev. B **25**, 1109 (1982).
[20]G. L. Zhao, T. C. Leung, B. N. Harmon, M. Keil, M. Muller, and W. Weber, Phys. Rev. B **40**, 7999 (1989).
[21]G. L. Zhao and B. N. Harmon, Phys. Rev. B **45**, 2818 (1992).
[22]J. G. Tobin, C. G. Olson, G. Gu, J. Z. Liu, F. R. Solal, M. J. Fluss, R. H. Howell, J. C. O'Brien, H. B. Radousky, and P. A. Sterne, Phys. Rev. B **45**, 5563 (1992).
[23]R. Liu, B. W. Veal, A. P. Paulikas, J. W. Downey, P. J. Kostic, S. Fleshler, U. Welp, C. G. Olson, X. Wu, A. J. Arko, and J. J. Joyce, Phys. Rev. B **46**, 11 056 (1992).
[24]N. Schroder, R. Böttner, S. Ratz, E. Dietz, U. Gerhardt, and Th. Wolf, Phys. Rev. B **47**, 5287 (1993).
[25]J. Humlicek, A. P. Litvinchuk, W. Kress, B. Lederle, C. Thomsen, M. Cardona, H. U. Habermeier, J. E. Trofimov, and W. Konig, Physica C **206**, 345 (1993).
[26]J. C. Slater and G. F. Koster, Phys. Rev. **94**, 1498 (1954).
[27]J. P. Carbotte, in *Anisotropy Effects in Superconductors,* edited by H. W. Weber (Plenum, New York, 1977), p. 183. We have inserted appropriate band indices.
[28]M. A. Beno, L. Soderholm, D. W. Capone II, D. G. Hinks, J. D. Jorgensen, I. K. Schuller, C. Segre, and J. D. Grace, Appl. Phys. Lett. **51**, 57 (1987).
[29]W. Reichardt, N. Pyka, L. Pintschovius, B. Hennion, and G. Collin, Physica C **162-164**, 464 (1989).
[30]T. Jarlborg, Solid State Commun. **67**, 297 (1988).
[31]R. Zeyher, Z. Phys. B **80**, 187 (1990).
[32]H. Krakauer, W. E. Pickett, and R. E. Cohen, Phys. Rev. B **47**, 1002 (1993).
[33]J. H. Nickel, D. E. Morris, and J. W. Ager, Phys. Rev. Lett. **70**, 81 (1993).
[34]G. D. Mahan, Phys. Rev. Lett. **71**, 4277 (1993); Phys. Rev. B **48**, 16 557 (1993); **40**, 11 317 (1989).
[35]E. T. Heyen, M. Cardona, J. Karpinski, E. Kaldis, and S. Rusieki, Phys. Rev. B **43**, 12 958 (1991); K. F. McCarty, J. Z. Liu, R. N. Shelton, and H. R. Radousky, *ibid.* **42**, 9973 (1990); K. F. McCarty, H. B. Radousky, J. Z. Liu, and R. N. Shelton, *ibid.* **43**, 13 751 (1991).
[36]M. Gurvich, J. M. Valles, Jr., A. M. Cucold, R. C. Dynes, J.P. Gamo, L. F. Schneemeyer, and J. V. Waszczak, Phys. Rev. Lett. **63**, 1008 (1989); V. Z. Kresin and S. A. Wolf, Physica C **169**, 476 (1990).
[37]S. E. Barett, D. J. Durand, C. H. Pennington, C. P. Slichter, T. A. Friedmann, J. P. Rice, and D. M. Ginsberg, Phys. Rev. B **41**, 6283 (1990).
[38]P. Vashishta and J. P. Carbotte, Phys. Rev. B **7**, 1874 (1973).
[39]J. H. Kim, K. Levin, R. Wentzcovitch, and A. Auerbach, Phys. Rev. B **44**, 5148 (1991).
[40]H. Chen, J. Callaway, N. E. Brener, and Z. Zou, Phys. Rev. B **43**, 383 (1991).